IEEE Access
Multidisciplinary | Rapid Review | Open Access Journal

Received September 28, 2019, accepted October 17, 2019, date of publication October 21, 2019, date of current version November 1, 2019.

Digital Object Identifier 10.1109/ACCESS.2019.2948639

Dual-Band Eight-Element MIMO Array Using Multi-Slot Decoupling Technique for 5G Terminals

WEI HU[1], (Member, IEEE), LONG QIAN[1], STEVEN GAO[2], (Fellow, IEEE), LE-HU WEN[2], QI LUO[2], (Member, IEEE), HANG XU[3], XUEKANG LIU[1], YING LIU[1], (Senior Member, IEEE), AND WEI WANG[4]

[1]National Laboratory of Science and Technology on Antennas and Microwaves, Xidian University, Xi'an 710071, China
[2]School of Engineering and Digital Arts, University of Kent, Canterbury CT2 7NT, U.K.
[3]Huawei Technologies Company Ltd., Shenzhen 518129, China
[4]East China Research Institute of Electronic Engineering, Hefei 230088, China

Corresponding authors: Wei Hu (weihu.xidian@ieee.org) and Long Qian (qianlong@stu.xidian.edu.cn)

This work was supported in part by the Young Talent Fund of University Association for Science and Technology in Shaanxi, China, under Grant 20170105, in part by the Natural Science Foundation of Shaanxi, China, under Grant 2018JM6038, in part by the Engineering and Physical Sciences Research Council (EPSRC) under Grant EP/N032497/1, Grant EP/P015840/1, and Grant EP/S005625/1, and in part by the Fundamental Research Funds for the Central Universities under Grant RC1902.

ABSTRACT This paper presents a dual-band eight-element multiple-input multiple-output (MIMO) array using a multi-slot decoupling technique for the fifth generation (5G) mobile communication. By employing a compact dual-loop antenna element, the proposed array obtains two broad bandwidths of 12.2% and 15.4% for sub-6GHz operation. To reduce the mutual coupling between antenna elements, a novel dual-band decoupling method is proposed by employing a multi-slot structure. The proposed MIMO array achieves 15.5-dB and 19.0-dB isolations across the two operating bands. Furthermore, three decoupling modes generated by different bent slots can be independently tuned. Zero ground clearance is also realized by the coplanar arrangement of the antenna elements and decoupling structures. The proposed MIMO array was simulated, fabricated, and measured. Experimental results agree well with the simulations, showing that the dual-band MIMO array has good impedance matching, high isolation, and high efficiency. In addition, the envelope correlation coefficient and channel capacity are calculated and analyzed to validate the MIMO performance of the 5G terminal array. Such a dual-band high-isolation eight-element MIMO array with zero ground clearance is a promising candidate for 5G or future mobile applications.

INDEX TERMS Dual-band decoupling, fifth generation (5G) communication, MIMO antenna, smartphone antenna.

I. INTRODUCTION

With the rapid evolution of mobile communication technologies, the fifth generation (5G) wireless systems have been attracting an increasing interest in recent years, due to their advantages of large channel capacity, high spectral efficiency, and massive connection density [1]. As one of the key technologies of 5G communication systems, multiple-input multiple-output (MIMO) technology is utilized to effectively increase the channel capacity in rich scattering environments [2]. The challenge for the terminal antenna design is that there is very limited space for multi-element MIMO array in today's mobile devices, as more and more communication standards are required to be integrated into a single system. Therefore, it is necessary to investigate MIMO antennas with compact size, multiple bandwidths, and high isolation [3].

Recently, many MIMO terminal antenna designs were reported [4]–[12]. Compact gap-coupled antenna pairs for eight-element MIMO array was proposed in [5], which operates at the 3.5-GHz band with 10-dB isolation. Similar asymmetrically mirrored structure is also used in [6], which obtains 3.5/5.8GHz dual-band operating performance. By using T-shaped coupled-fed slot elements [8], a ten-element array for sub-6 GHz operation was designed with isolation of 10 dB and 12.5 dB over the two bands.

The associate editor coordinating the review of this manuscript and approving it for publication was Pietro Savazzi.

In [11], a platform-free planar inverted-F antenna (PIFA) array with 7% and 8% bandwidths for 5G MIMO applications was reported. This array can be compatible with different platforms by adding vertical patches. Besides, an ultra-wideband four-element MIMO array is studied in [12], which can cover 3300-6000MHz with 10-dB isolation. For multi-element MIMO array, it is challenging to achieve low mutual coupling in the limited area. To solve this problem, various decoupling techniques have been used in 5G terminals, such as the orthogonal mode [13]–[15], balanced slot mode [16], grounded strips [17], pattern diversity [18], [19], neutralization line [20], [21], and inherent decoupling structure [22], [23]. A tightly-arranged array based on orthogonal mode method was developed in [15]. The isolation of the 8×8 MIMO system is better than 17 dB across the operating band. In [16], by combining two decoupling techniques of the balanced slot mode and polarization diversity, an eight-element array realized 17.5-dB isolation in the 3.5-GHz band. In [17], by inserting a metal ground between the decoupling shorting strips, the resonant frequencies of the decoupling strips can be tuned independently. A pattern-diversity-based decoupling method without any decoupling structure was presented in [18], and more than 15-dB isolation is obtained in the eight-element array. In [20], by introducing the neutralization lines into the middle elements of a dual-band MIMO array, the isolation was improved by 3 dB at the 3.5-GHz band. In [23], a dual-band dual-element MIMO array is studied. By using the proposed inherent decoupling structures, good isolation can be obtained in both two frequency bands. These reported decoupling techniques can realize a reduction of the mutual coupling for terminal antennas. However, it is difficult to improve the isolation for 5G multi (eight or more) elements dual-band MIMO array.

In this paper, a novel multi-slot dual-band decoupling technique is proposed to enhance the isolation of a dual-loop antenna array for 5G MIMO terminals. In this design, a compact dual-loop antenna element is developed for dual-band sub-6 GHz operation. Dual resonances are generated by two different split loops, which produce two wide operating bands of 12.2% and 15.4%, respectively. To obtain low mutual coupling within the limited space of 5G terminals, a new dual-band decoupling technique is proposed by employing a multi-slot structure. Three bent slots produce different decoupling modes with independent tuning characteristic at desirable frequencies to improve the isolation in the lower and higher bands simultaneously. Moreover, thanks to the coplanar design of antenna elements and decoupling structures on the side edges, zero ground clearance is realized in the proposed MIMO array, which is promising to place this design along a narrow region and reserve more space for other electronic components.

To validate the design concept, the proposed dual-band eight-element array is designed, fabricated, and measured. The measured results show that the proposed MIMO array achieves the 15.5-dB and 19-dB isolations across the two operating bands. The antenna efficiencies of 42%–83% in the lower band and 40%–85% in the higher band are obtained. Low envelope correlation coefficients (ECCs) and high channel capacities are achieved within the two bands, which indicate the proposed eight-element array can have a good MIMO performance for the dual-band 5G terminal applications.

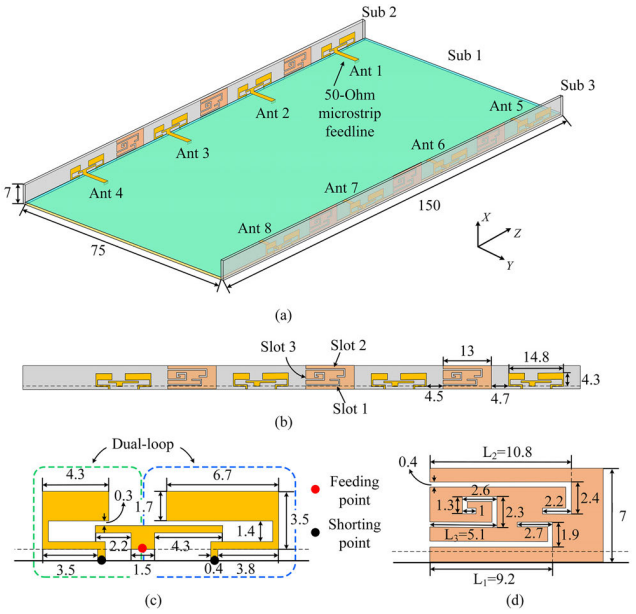

FIGURE 1. Configuration of the proposed eight-element array. (a) Overall view. (b) Side view. Detailed geometries of (c) the antenna element and (d) the decoupling structure with dimensions in millimeters.

II. DUAL-BAND MIMO ARRAY USING MULTI-SLOT DECOUPLING TECHNIQUE

A. MIMO ARRAY CONFIGURATION

The configuration of the proposed dual-band eight-element array for 5G MIMO terminal applications is shown in Fig. 1. There are three printed circuit boards (PCBs) in the design, including Sub 1, Sub 2, and Sub 3. All of them are 0.8 mm-thick FR-4 substrates (relative permittivity of 4.65, loss tangent of 0.02). Sub 1 is employed as the system circuit board for a 5.5-inch mobile terminal with a size of 150 mm × 75 mm. The 50-Ohm microstrip feedlines and metal ground plane are printed on the top and bottom layers of Sub 1, respectively. Sub 2 and Sub 3 have the same size of 150 mm × 7 mm, which are perpendicularly placed along the two side edges of Sub 1. On the inner sides of Sub 2 and Sub 3, the antenna elements and decoupling structures are symmetrically arranged along the two long edges of the system circuit board.

The dual-loop antenna elements have a compact size of 14.8 mm × 4.3 mm, which are placed at the same distance of 22.2 mm (0.25λ at 3.4 GHz) between the edges of adjacent antenna elements. As shown in Fig. 1(c), the proposed antenna element is composed of two folded strips and a T-shaped feeding line, which form two split loops. Multi-slot decoupling structures are designed on the same layer as the

antenna elements. As shown in Fig. 1(d), three bent slots with an identical width of 0.4 mm are embedded on a grounded patch with a size of 13 mm × 7 mm. Note that there is no need of any ground clearance for this design as it is realized by using a coplanar arrangement of the antenna elements and decoupling structures on the side edges.

B. DUAL-BAND DUAL-LOOP ANTENNA ELEMENT

The proposed antenna consists of two split loops with different lengths, which are formed by two folded strips and a T-shaped coupled feedline. Fig. 2 shows the simulated $|S_{11}|$ of the antenna element (Ant 1). The simulation was performed by using ANSYS High-Frequency Structure Simulator (HFSS). The −6-dB impedance bandwidths are 500 MHz (3.34–3.84 GHz) and 850 MHz (4.66–5.51GHz), which covers the sub-6 GHz 5G frequency bands, as well as WLAN and WiMAX. The simulated input impedance for the Ant 1 is shown in Fig. 3. It can be seen that two resonances are generated at 3.6 GHz and 4.9 GHz, and good impedance matching is obtained in both desired bands. This result is in good agreement with the simulated result of $|S_{11}|$ shown in Fig. 2.

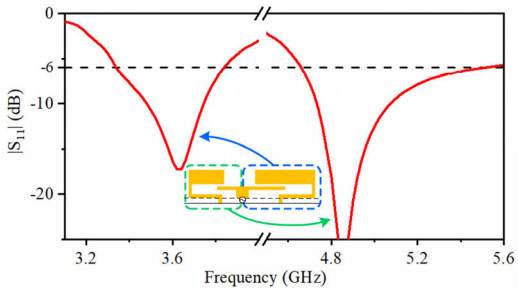

FIGURE 2. Simulated $|S_{11}|$ of the antenna element (Ant 1).

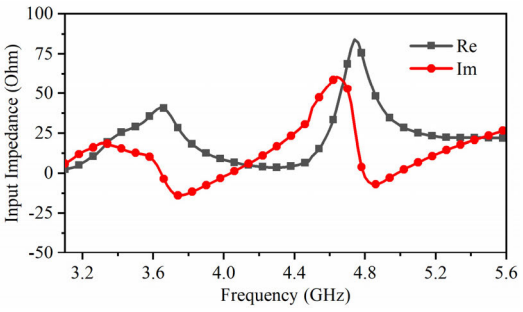

FIGURE 3. Simulated input impedance of the antenna element (Ant 1).

To investigate the dual-band operation mechanism of the proposed antenna element, the simulated surface current distributions at 3.6 GHz and 4.9 GHz are shown in Fig. 4. The electromagnetic energy is coupled from the T-shaped feeding structure to the open ends of two folded strips. At 3.6 GHz, the surface current is concentrated along the loop path of ABCD of Ant 1. While at 4.9 GHz, strong surface current density is observed on the loop path of AEFG. Total lengths of coupling

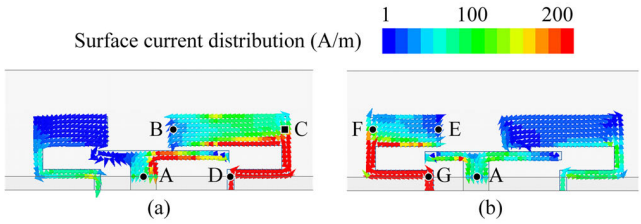

FIGURE 4. Simulated surface current distributions of the antenna element (Ant 1) at (a) 3.6 GHz and (b) 4.9 GHz.

loop paths ABCD and AEFG are 20.1 mm and 17.6 mm, which are corresponding to the quarter free-space wavelength at 3.6 GHz and 4.9 GHz, respectively. Therefore, the dual-loop antenna can generate two independent resonances for the dual-band operation. By employing capacitively coupling, the proposed dual-loop antenna design achieves a compact size and two wide bandwidths, as compared with the traditional loop antennas using half-wavelength modes [24]–[26].

C. DUAL-BAND MULTI-SLOT DECOUPLING STRUCTURE

For MIMO antenna array in sub-6 GHz bands, it is challenging to obtain low mutual coupling within a limited space. In this work, a multi-slot decoupling structure is developed to obtain dual-band high isolation between the antenna elements. Three different bent slots are embedded on a grounded patch, and its occupied area is only 13 mm × 7 mm on the side edges. Thanks to the coplanar design with the antenna elements, the decoupling structures do not occupy any extra ground.

To illustrate the effect of the multi-slot decoupling technique, the simulated S-parameters of the proposed antenna array (Ant 1–Ant 4) with and without the decoupling structures are shown in Fig. 5. The results of Ant 5–Ant 8 are not given for brevity due to the symmetric layout of the eight-element array. As shown in Fig. 5(a), when the antenna array is without the decoupling structures, the port isolation in the lower and higher bands are only 11.5 dB and 12.5 dB, respectively. Owing to the strong mutual coupling between adjacent elements, the antenna impedance bandwidths are deteriorated in the lower band, which can only cover 3.43–3.67GHz.

In order to improve the dual-band isolation of the antenna array, multiple decoupling slots are introduced on a rectangular metal patch, which is vertically connected to the ground plane. By employing three bent slots with different lengths, the presented decoupling structure generates three decoupling modes to reduce the mutual coupling both in the lower and higher bands. As shown in Fig. 5(b), three decoupling modes, Slot-1, Slot-2, and Slot-3 modes are obtained at 3.2 GHz, 3.4 GHz, and 4.8 GHz, respectively. By using the multi-slot decoupling structures, the dual-band isolations are enhanced from 11.5 dB to 16 dB in the lower band and from 12.5 dB to 19 dB in the higher band. Moreover, all the antenna elements can operate over the 3.40–3.84 GHz and

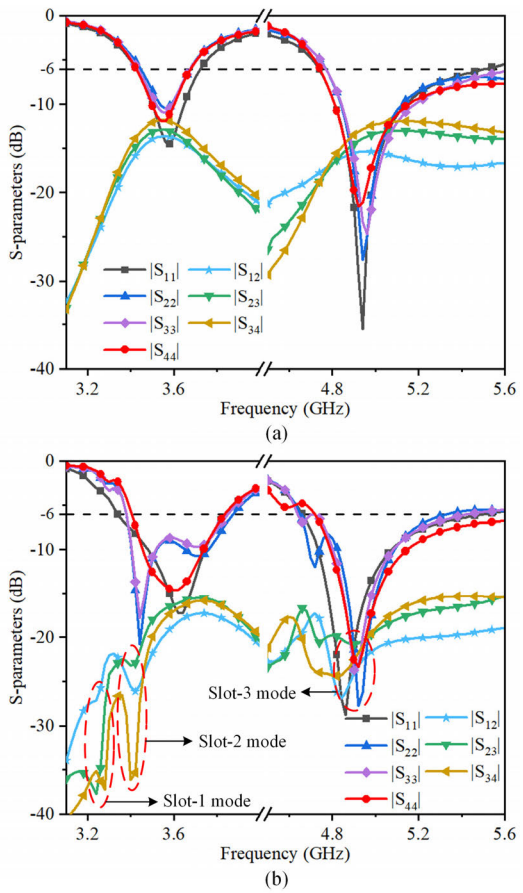

FIGURE 5. Simulated S-parameters of the antenna array (a) without and (b) with the multi-slot decoupling structure.

4.72–5.33 GHz frequency ranges for dual-band 5G terminal applications.

To investigate the multi-slot decoupling technique, different decoupling structures involved in the design evolution process are shown in Fig. 6. As shown in Fig. 6(a), when there is only the rectangular metal patch connected to the ground without the decoupling slots, the transmission coefficients of the antenna elements are almost not affected by the grounded patch. Then, the slot 1 is introduced into the lower half of the patch, as shown in Fig. 6(b). This can excite a decoupling mode at 3.2 GHz to improve the isolation between antenna elements from 11.5 dB to 13.5 dB in the lower band. To further enhance isolation in the lower frequency band, Slot 2 is embedded into the upper half of the grounded patch. As shown in Fig. 6(c), an additional decoupling mode appears at 3.4 GHz. After combining the Slot-1 and Slot-2 modes, a good isolation level of 16 dB is achieved in the lower band. To reduce the mutual coupling in the higher band, Slot 3 is inserted between Slot 1 and Slot 2, which produces a decoupling mode at 4.8 GHz. The isolation of 19 dB is obtained in the higher band as plotted in Fig. 6(d). In this way, three decoupling slots can be appropriately arranged to reduce the mutual coupling effect between the antenna elements for dual-band sub-6 GHz operation. The design of the decoupling structure involves the following two steps: (1) introducing Slot 1 and Slot 2 to reduce the effect of mutual coupling in the lower band. (2) introducing Slot 3 to reduce the effect of mutual coupling in the higher band.

To further illustrate the operating mechanism of the dual-band multi-slot decoupling technique, Fig. 7 shows the simulated surface current distributions of Ant 1 and Ant 2 with and without the decoupling structure when Ant 1 is excited. As shown, without the decoupling structures, strong currents are coupled from Ant 1 to Ant 2 at the two resonant frequencies of the dual-loop antenna. This leads to poor isolation between the antenna elements. By introducing the multi-slot decoupling structure between the Ant 1 and Ant 2, the strong current density is observed on the Slot 1 and Slot 2 at 3.6 GHz in the lower band, as shown in Fig. 7(a). Similarly, it also can be seen the surface current

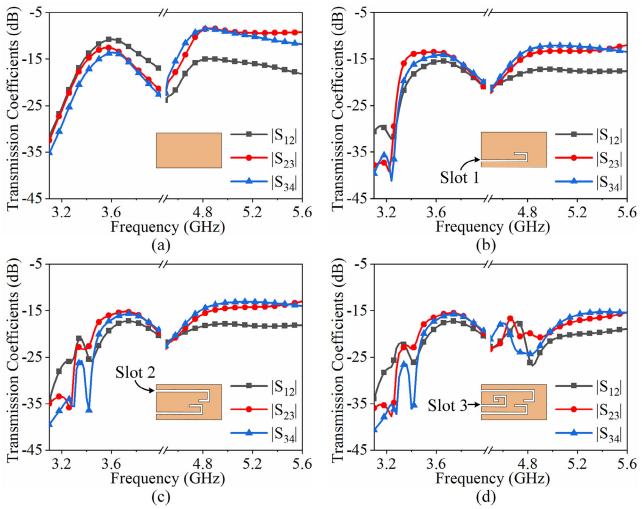

FIGURE 6. Simulated transmission coefficients of the different decoupling structure involved in the design evolution process. (a) Without slots, (b) with Slot 1, (c) with Slot 1 and Slot 2, and (d) with Slot 1, Slot 2, and Slot 3.

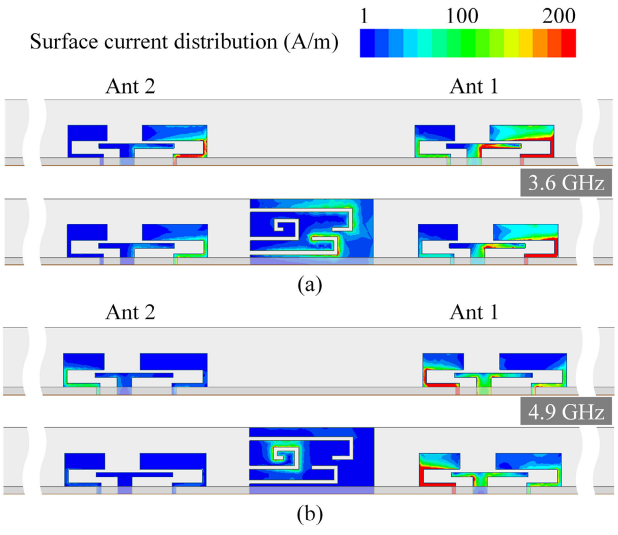

FIGURE 7. Simulated surface current distributions of Ant 1 and Ant 2 without and with the decoupling structure at (a) 3.6 GHz and (b) 4.9 GHz.

distributions are concentrated on the Slot 3 at 4.9 GHz in the higher band, as shown in Fig. 7(b). There is very weak energy coupled from Ant 1 to Ant 2 at the lower and higher center frequencies, which means that the multi-slot decoupling structure can effectively reduce the mutual coupling between the antenna elements. The observed current distributions are consistent with the design concept, which validates the proposed dual-band multi-slot decoupling approach.

Fig. 8 shows the simulated $|S_{12}|$ of the antenna array for various lengths of the three decoupling slots. In Fig. 8(a), it can be seen that the first decoupling mode can be manipulated by changing the length L_1 of Slot 1, when L_2 and L_3 are fixed. Meanwhile, there is little effect on the Slot-2 and Slot-3 modes. Similar operating characteristics of Slot 2 and Slot 3 are also observed in Fig. 8(b) and (c), respectively. Thereby, it can be concluded that three decoupling modes can be controlled independently by adjusting the lengths of the corresponding slots.

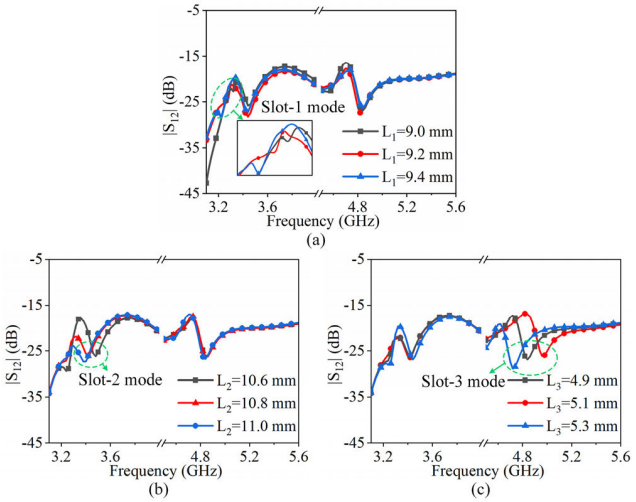

FIGURE 8. Simulated $|S_{12}|$ of the antenna array for various (a) L_1, (b) L_2, and (c) L_3.

D. ANTENNA EFFICIENCY

As a key figure of merit for 5G MIMO array design, the antenna total efficiency should be considered for a multi-element array. Therefore, the simulated antenna efficiencies of the proposed antenna array with and without the decoupling structures are shown in Fig. 9. As can be seen in Fig. 9(a), in the lower band, the simulated antenna efficiencies are worse than that in Fig. 9(b). This is mainly because the MIMO array has a narrower impedance bandwidth compared with the array using decoupling structures, as shown in Fig. 5. By introducing the proposed multi-slot decoupling structures, the antenna efficiencies are improved from 28% to 40% in the lower band. Meanwhile, 50% antenna efficiencies in the higher band are also obtained. In this array design, the resonant frequency of the decoupling modes is slightly deviated from the resonant frequency of the antenna to avoid the unstable efficiency in the lower band. Fig. 10 shows

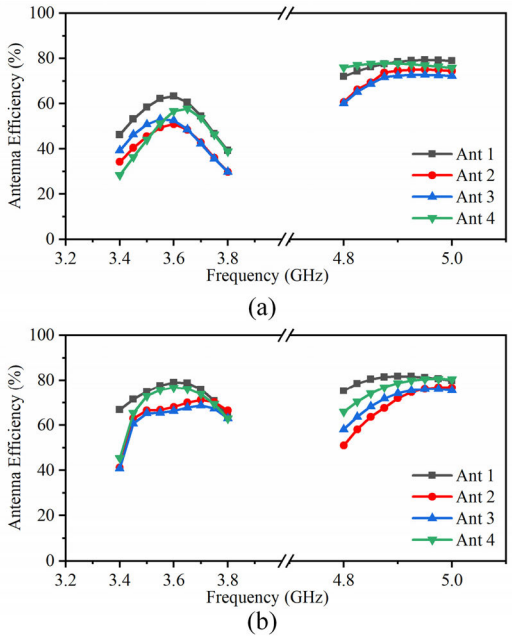

FIGURE 9. Simulated antenna efficiencies of the proposed antenna array (a) without and (b) with the decoupling structures.

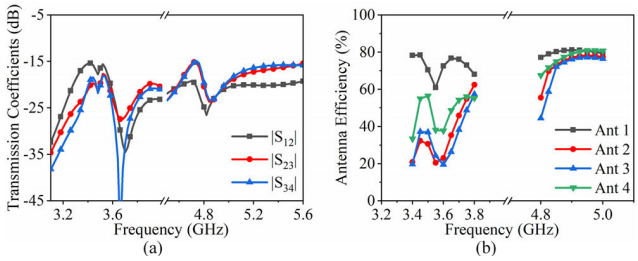

FIGURE 10. (a) Simulated transmission coefficients and (b) antenna efficiencies while the decoupling modes are excited at 3.5 GHz, 3.7 GHz, and 4.8 GHz.

the simulated transmission coefficients and antenna efficiencies when the decoupling modes are designed at 3.5 GHz, 3.7 GHz, and 4.8 GHz. It can be seen that in this case, isolation better than 15 dB is obtained in the lower band. However, the antenna elements suffer unstable efficiencies in the lower band, and Ant 3, Ant 4 only have 20% total efficiencies at 3.4 GHz. Therefore, the MIMO array using the presented decoupling structures can realize a good dual-band operating performance with total efficiency of more than 40% over both frequency bands.

III. RESULTS AND DISCUSSION

A. S-PARAMETERS

To validate the design concept, a dual-band eight-element array using the multi-slot decoupling technique was fabricated and measured. Fig. 11 shows the photographs of the fabricated eight-element array. The eight antenna elements with six decoupling structures are symmetrically arranged along the two side edges. Each antenna element is fed by a

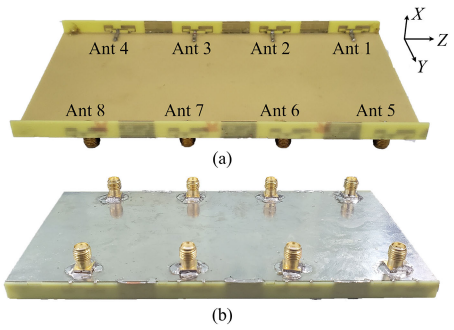

FIGURE 11. Photographs of the fabricated eight-element array. (a) Front view. (b) Back view.

50-Ohm SMA connector, which is mounted below the system circuit board.

The measured S-parameters are plotted in Fig. 12. Because of the symmetric layout of the eight-element array, only the results of Ant 1–Ant 4 are shown. As can be seen, the experimental results agree well with the simulated ones in Fig. 4(b). By using the proposed dual-loop antenna elements, two resonances are excited with a good impedance matching of 440 MHz (3.38–3.82 GHz) and 800 MHz (4.80–5.60 GHz) under the criterion of less than −6-dB reflection coefficient. Furthermore, high isolations between antenna elements are obtained, which are better than 15.5 dB and 19 dB in the lower and higher bands, respectively.

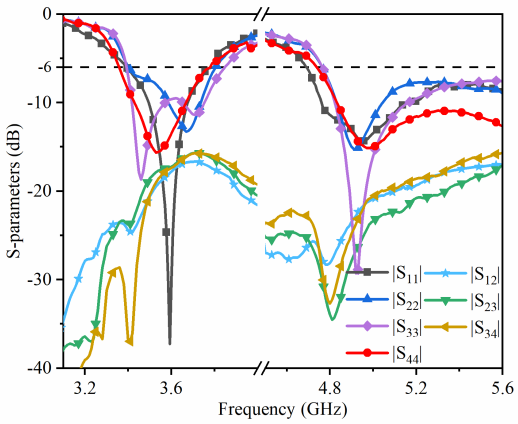

FIGURE 12. Measured S-parameters of the proposed antenna array.

B. RADIATION PERFORMANCES

Figs. 13 and 14 show the simulated and measured normalized radiation patterns in *xy*-plane at 3.6 GHz and 4.9 GHz, respectively. Due to the symmetrical array layout, only radiation patterns of Ant 1–Ant 4 are given in the figure for brevity. As can be observed, the measured radiation patterns agree reasonably well with the simulated results at the two operating frequencies. The radiation performance measurements were carried out in a near-field antenna measurement system at Xidian University. The measured antenna total efficiencies

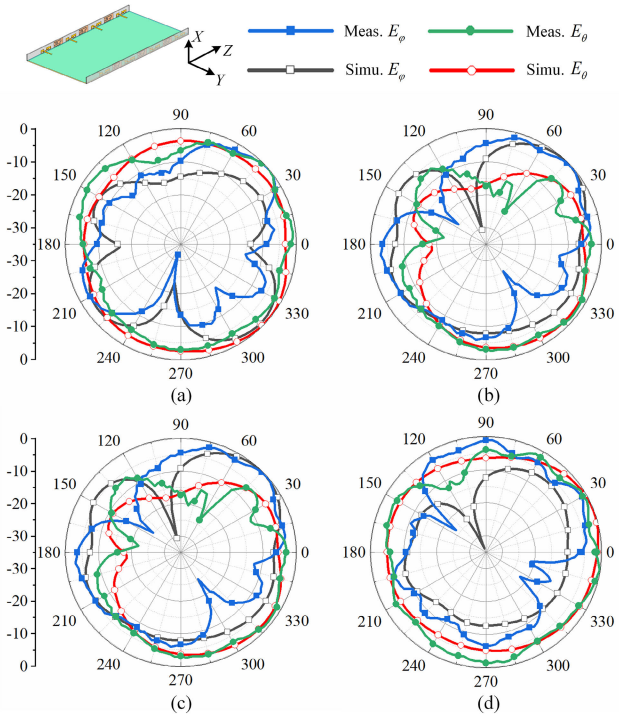

FIGURE 13. Simulated and measured normalized radiation patterns in the xy-plane of the different antenna elements at 3.6 GHz. (a) Ant 1. (b) Ant 2. (c) Ant 3. (d) Ant 4.

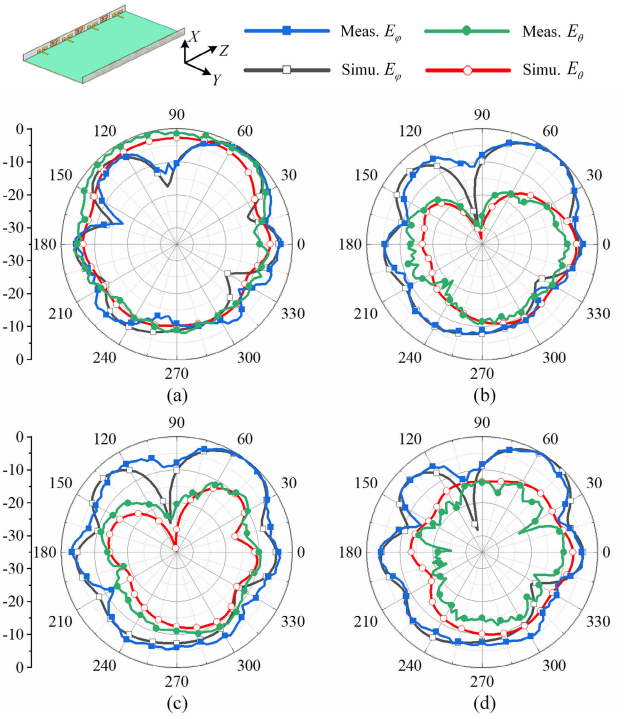

FIGURE 14. Simulated and measured normalized radiation patterns in the xy-plane of the different antenna elements at 4.9 GHz. (a) Ant 1. (b) Ant 2. (c) Ant 3. (d) Ant 4.

of the four representative antenna elements (Ant 1–Ant 4) are presented in Fig. 15. It can be seen that the measured antenna efficiencies are about 42%–83% in the lower band, and 40%–85% in the higher band. The experimental results

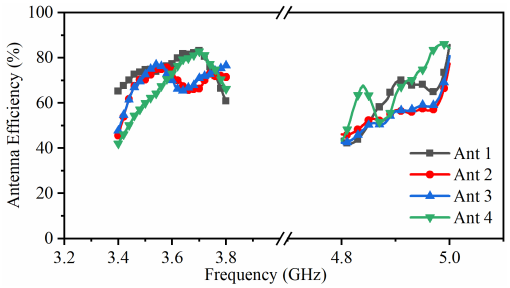

FIGURE 15. Measured antenna efficiencies of the proposed antenna array.

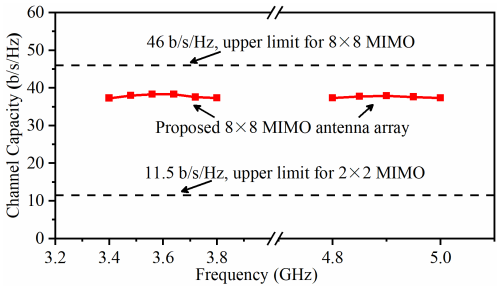

FIGURE 17. Calculated ergodic channel capacities of the fabricated antenna array.

indicate the proposed eight-element array achieves good radiation performances in the two operating bands, which are suitable for the practical MIMO terminal operation.

C. MIMO PERFORMANCES

To evaluate the potential MIMO performance of the proposed antenna array, the ECCs and channel capacities are calculated and analyzed. Fig. 16 shows the results of ECCs of Ant 1–Ant 2, Ant 2–Ant 3, and Ant 3–Ant 4, which are calculated from the measured radiation patterns [27] and S-parameters. It can be seen in Fig. 16(a) that the ECCs are less than 0.07 and 0.06 in the lower and higher bands respectively, which is in good agreement with the results calculated by the measured S-parameters. Both the results guarantee a good diversity performance of the MIMO antenna array. Besides, the calculated ergodic channel capacities of the fabricated eight-element array are shown in Fig. 17. The channel capacities with a 20-dB SNR vary from 37.3 to 38.3 b/s/Hz in the two bands, which are 3.2 times larger than the upper limit of a 2×2 MIMO system. Compared with the upper limit of 46 b/s/Hz for an 8×8 MIMO antennas, the proposed array exhibits desirable channel capacities that are only 8 b/s/Hz less than the ideal case. Therefore, based on the calculated ECC and channel capacities, the proposed dual-band eight-element array is capable of providing good MIMO performances for 5G terminal applications.

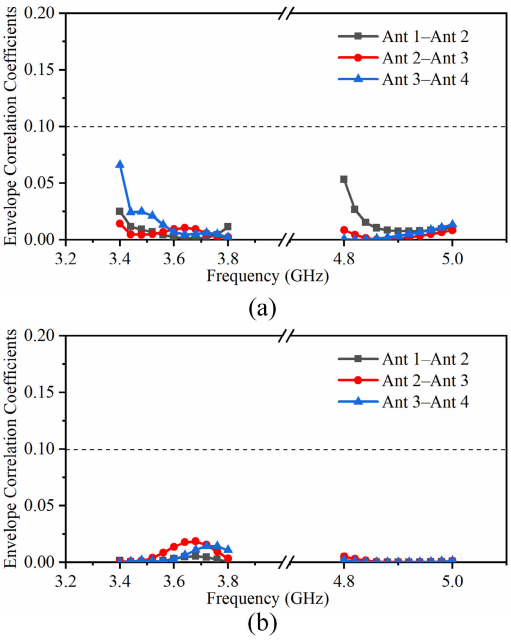

FIGURE 16. Calculated ECCs of the fabricated antenna array from the measured (a) radiation patterns and (b) S-parameters.

D. USER'S HAND EFFECTS

To investigate the operating performance of the antenna array in practical scenarios, the effects of the user's hand are studied in the subsection. As shown in Fig. 18, there are two typical 5G usage scenarios, the single-hand operation (SHO) and dual-hand operation (DHO).

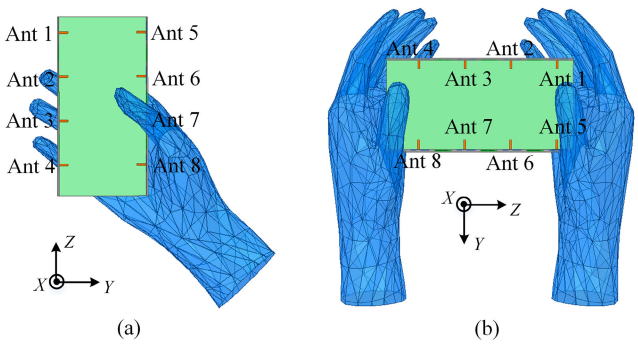

FIGURE 18. Two typical usage scenarios under user's hand operation. (a) SHO mode. (b) DHO mode.

Figs. 19 and 20 show the simulated reflection coefficients, transmission coefficients, and antenna total efficiencies of the proposed array in the SHO mode and DHO mode, respectively. For the SHO mode, it can be seen in Fig. 19(a) that the reflection coefficients of the proposed array are not affected drastically by the hand, except for some small frequency fluctuations at the edges of the working band. In Fig. 19(b), the isolation between antenna elements becomes better with the hold of the hand. This is because some EM energy has been absorbed by the hand. However, the antenna efficiencies of the proposed array are affected significantly owing to the absorption effect of the user's hand. As shown in Fig. 19(c), the antenna efficiencies of Ant 2, Ant 7, and Ant 8 are declined to 18% because they are very close to the hand. For DHO mode, a similar phenomenon can be observed

TABLE 1. Comparison between the proposed design and the referenced antennas for 5G terminal applications.

Ref.	Impedance bandwidth (-6-dB)	Covering bands (GHz)	Isolation (dB)	Total efficiency (%)	ECC	MIMO order	Ground clearance (mm)	Decoupling technique
[4]	12%	3.4–3.6	>10	>62	<0.2	8	3	None
[5]	5.7%	3.4–3.6	>10	>40	<0.1	8	1	None
[6]	8.5%, 16.7%	3.4–3.6, 5.725–5.925	>14, >11	42–60, 65–80	<0.15, <0.15	8	1	None
[8]	11.1%, 14.0%	3.4–3.8, 5.15–5.925	>10.0, >12.5	42–65, 62–82	<0.15, <0.05	10	3	None
[15]	5.7%	3.4–3.6	>17	49–73	<0.07	8	1	Single-band Orthogonal mode
[16]	11.4%*	3.4–3.6	>17.5	62–76	<0.04	8	1	Single-band Balanced slot mode & Polarization diversity
[20]	5.7%, 6.1%	3.4–3.6, 4.8–5.0	>11.5, >15.0	41–72, 40–85	<0.08, <0.05	8	1	Single-band Neutralization line
[23]	9.9%, 28.6%	2.40–2.48, 5.15-5.35, 5.725–5.925	>20, >15	44–48, 74–80	<0.14, <0.05	2	1	Dual-band Inherent decoupling structures
This work	12.2%, 15.4%	3.4–3.8, 4.8–5.0	>15.5, >19.0	42–83, 40–85	<0.07, <0.06	8	0	Dual-band Multiple slots

* The value is extracted from the measured reflection coefficients given in the original reference.

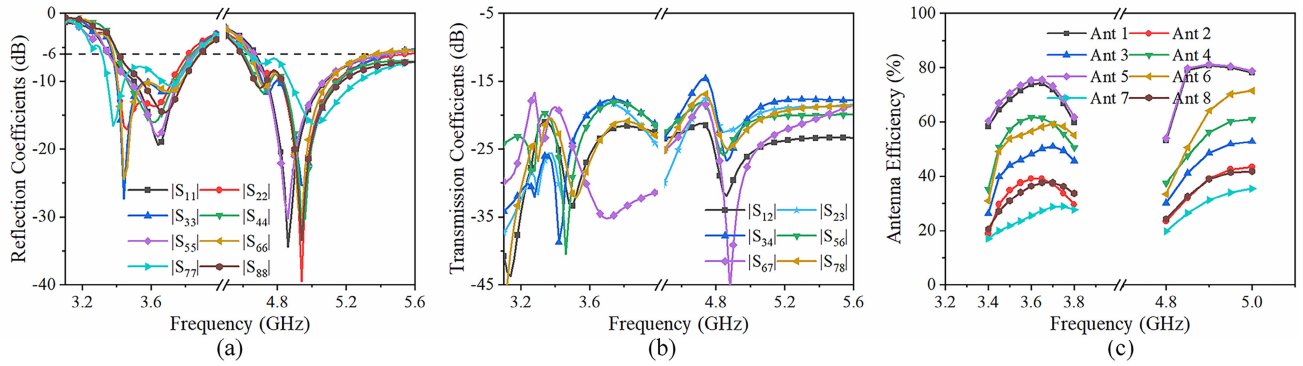

FIGURE 19. Simulated (a) reflection coefficients, (b) transmission coefficients, and (c) antenna efficiencies of the proposed eight-element array in SHO mode.

in Fig. 20. The reflection coefficients and the isolations have little deterioration. The eight-element array can still cover the two working bands with the two hands holding. Meanwhile, the antenna efficiency decreases significantly due to the absorption effect of the hands. The antenna efficiencies of only 17% are obtained in DHO mode.

E. COMPARISON

Table 1 compares the presented design with the recently reported 5G terminal MIMO antennas. To the best knowledge of the authors, most of the reported antennas for sub-6 GHz 5G terminals are single-band operating, and there are few reported works on the use of the dual-band decoupling technique for multi-element terminal systems. The designs reported in [4], [5], [15] and [16] are the single-band antennas operating at the 3.5-GHz band. Compared with these designs, the proposed design shows two wider operating bandwidths with comparable isolation level and total efficiency. In [6], [8] and [20], the reported MIMO antennas are of dual-band operation. Compared with these three designs, the presented antenna array exhibits much higher isolations with comparable total efficiency. The reported MIMO antenna in [23] consists of only two antenna elements for dual-band operation. Compared with this design, the proposed MIMO antenna array has a larger MIMO order and higher channel capacity. It should be noted that most of the reported mobile MIMO antennas require some ground clearance. The presented MIMO array does not need any ground clearance, and this allows it to be placed along a narrow region and reserved more space for other electronic components.

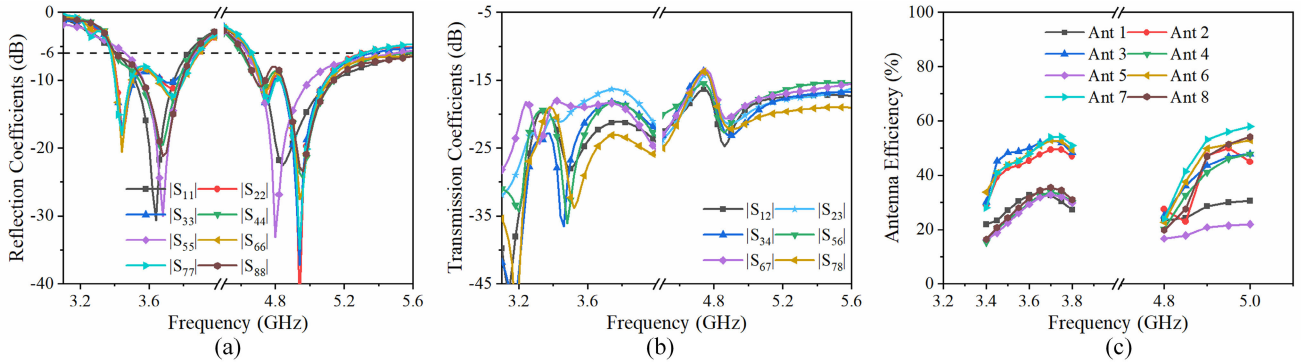

FIGURE 20. Simulated (a) reflection coefficients, (b) transmission coefficients, and (c) antenna efficiencies of the proposed eight-element array in DHO mode.

IV. CONCLUSION

A novel method to design a dual-band MIMO array using the multi-slot decoupling technique is presented in this paper. The proposed terminal array is composed of eight compact dual-loop antenna elements, which can generate two quarter-wavelength resonances with 12.2% and 15.4% bandwidths, respectively. To obtain low mutual coupling within a limited space, a new multi-slot structure is introduced between the antenna elements. High isolations of 15.5 dB and 19.0 dB are achieved in the two sub-6 GHz operating bands. To validate the design concept, the MIMO array prototype was fabricated and measured. Good agreement is obtained between the simulated and the measured results. Owing to the dual wideband, high isolation, zero ground clearance, high efficiency, large channel capacity, and low ECC level, the proposed eight-element array can be a desirable candidate for 5G and future MIMO terminal applications.

REFERENCES

[1] K. M. Mak, H. W. Lai, K. M. Luk, and C. H. Chan, "Circularly polarized patch antenna for future 5G mobile phones," *IEEE Access*, vol. 2, pp. 1521–1529, 2014.

[2] J. G. Andrews, S. Buzzi, W. Choi, S. V. Hanly, A. Lozano, A. C. K. Soong, and J. C. Zhang, "What will 5G be?" *IEEE J. Sel. Areas Commun.*, vol. 32, no. 6, pp. 1065–1082, Jun. 2014.

[3] W. Hong, "Solving the 5G mobile antenna puzzle: Assessing future directions for the 5G mobile antenna paradigm shift," *IEEE Microw. Mag.*, vol. 18, no. 7, pp. 86–102, Nov. 2017.

[4] Y.-L. Ban, C. Li, C.-Y.-D. Sim, G. Wu, and K.-L. Wong, "4G/5G multiple antennas for future multi-mode smartphone applications," *IEEE Access*, vol. 4, pp. 2981–2988, 2016.

[5] K.-L. Wong, C.-Y. Tsai, and J.-Y. Lu, "Two asymmetrically mirrored gap-coupled loop antennas as a compact building block for eight-antenna MIMO array in the future smartphone," *IEEE Trans. Antennas Propag.*, vol. 65, no. 4, pp. 1765–1778, Apr. 2017.

[6] K.-L. Wong, B.-W. Lin, and W.-Y. Li, "Dual-band dual inverted-F/loop antennas as a compact decoupled building block for forming eight 3.5/5.8-GHz MIMO antennas in the future smartphone," *Microw. Opt. Technol. Lett.*, vol. 59, no. 11, pp. 2715–2721, Nov. 2017.

[7] A. A. Al-Hadi, J. Ilvonen, R. Valkonen, and V. Viikari, "Eight-element antenna array for diversity and MIMO mobile terminal in LTE 3500 MHz band," *Microw. Opt. Technol. Lett.*, vol. 56, no. 6, pp. 1323–1327, Jun. 2014.

[8] Y. Li, C.-Y.-D. Sim, Y. Luo, and G. Yang, "Multiband 10-antenna array for sub-6 GHz MIMO applications in 5-G smartphones," *IEEE Access*, vol. 6, pp. 28041–28053, 2018.

[9] Z. Qin, W. Geyi, M. Zhang, and J. Wang, "Printed eight-element MIMO system for compact and thin 5G mobile handest," *Electron. Lett.*, vol. 52, no. 6, pp. 416–418, Feb. 2016.

[10] Y. Li, C.-Y.-D. Sim, Y. Luo, and G. Yang, "12-port 5G massive MIMO antenna array in Sub-6GHz mobile handset for LTE bands 42/43/46 applications," *IEEE Access*, vol. 6, pp. 344–354, 2017.

[11] D. Q. Liu, M. Zhang, H. J. Luo, H. L. Wen, and J. Wang, "Dual-band platform-free PIFA for 5G MIMO application of mobile devices," *IEEE Trans. Antennas Propag.*, vol. 66, no. 11, pp. 6328–6333, Nov. 2018.

[12] K.-L. Wong, Y.-H. Chen, and W.-Y. Li, "Decoupled compact ultra-wideband MIMO antennas covering 3300 6000 MHz for the fifth-generation mobile and 5 GHz-WLAN operations in the future smartphone," *Microw. Opt. Technol. Lett.*, vol. 60, no. 10, pp. 2345–2351, Oct. 2018.

[13] M.-Y. Li, Y.-L. Ban, Z.-Q. Xu, J.-H. Guo, and Z.-F. Yu, "Tri-polarized 12-antenna MIMO array for future 5G smartphone applications," *IEEE Access*, vol. 5, pp. 6160–6170, 2018.

[14] M.-Y. Li, Y.-L. Ban, Z.-Q. Xu, G. Wu, C.-Y.-D. Sim, K. Kang, and Z.-F. Yu, "Eight-port orthogonally dual-polarized antenna array for 5G smartphone applications," *IEEE Trans. Antennas Propag.*, vol. 64, no. 9, pp. 3820–3830, Sep. 2016.

[15] L. B. Sun, H. Feng, Y. Li, and Z. Zhang, "Compact 5G MIMO mobile phone antennas with tightly arranged orthogonal-mode pairs," *IEEE Trans. Antennas Propag.*, vol. 66, no. 11, pp. 6364–6369, Nov. 2018.

[16] Y. Li, C.-Y.-D. Sim, Y. Luo, and G. L. Yang, "High-isolation 3.5 GHz eight-antenna MIMO array using balanced open-slot antenna element for 5G smartphones," *IEEE Trans. Antennas Propag.*, vol. 67, no. 6, pp. 3820–3830, Jun. 2019. doi: 10.1109/TAP.2019.2902751.

[17] H. Xu, H. Zhou, S. Gao, H. Wang, and Y. Cheng, "Multimode decoupling technique with independent tuning characteristic for mobile terminals," *IEEE Trans. Antennas Propag.*, vol. 65, no. 12, pp. 6739–6751, Dec. 2017.

[18] C. F. Ding, X. Y. Zhang, C.-D. Xue, and C.-Y.-D. Sim, "Novel pattern-diversity-based decoupling method and its application to multielement MIMO antenna," *IEEE Trans. Antennas Propag.*, vol. 66, no. 10, pp. 4976–4985, Oct. 2018.

[19] X. Zhao, S. P. Yeo, and L. C. Ong, "Planar UWB MIMO antenna with pattern diversity and isolation improvement for mobile platform based on the theory of characteristic modes," *IEEE Trans. Antennas Propag.*, vol. 66, no. 1, pp. 420–425, Jan. 2018.

[20] J. L. Guo, L. Cui, C. Li, and B. H. Sun, "Side-edge frame printed eight-port dual-band antenna array for 5G smartphone applications," *IEEE Trans. Antennas Propag.*, vol. 66, no. 12, pp. 7412–7417, Dec. 2018.

[21] K. L. Wong, J.-Y. Lu, L.-Y. Chen, W.-Y. Li, and Y.-L. Ban, "8-antenna and 16-antenna arrays using the quad-antenna linear array as a building block for the 3.5-GHz LTE MIMO operation in the smartphone," *Microw. Opt. Technol. Lett.*, vol. 58, no. 1, pp. 174–181, Jan. 2016.

[22] K.-L. Wong, B.-W. Lin, and S.-E. Lin, "High-isolation conjoined loop multi-input multi-output antennas for the fifth-generation tablet device," *Microw. Opt. Technol. Lett.*, vol. 61, no. 1, pp. 111–119, Jan. 2019.

[23] K.-L. Wong, C.-Y. Tsai, and W.-Y. Li, "Integrated yet decoupled dual antennas with inherent decoupling structures for 2.4/5.2/5.8-GHz WLAN MIMO operation in the smartphone," *Microw. Opt Technol Lett.*, vol. 59, no. 9, pp. 2235–2241, 2017.

[24] Y. L. Ban, Y. F. Qiang, Z. Chen, K. Kang, and J. H. Guo, "A dual-loop antenna design for hepta-band WWAN/LTE metal-rimmed smartphone applications," *IEEE Trans. Antennas Propag.*, vol. 63, no. 1, pp. 48–58, Jan. 2015.
[25] Y.-W. Chi and K.-L. Wong, "Compact multiband folded loop chip antenna for small-size mobile phone," *IEEE Trans. Antennas Propag.*, vol. 56, no. 12, pp. 3797–3803, Dec. 2008.
[26] M. Zheng, H. Wang, and Y. Hao, "Internal hexa-band folded monopole/dipole/loop antenna with four resonances for mobile device," *IEEE Trans. Antennas Propag.*, vol. 56, no. 12, pp. 3797–3803, Jun. 2008.
[27] M. S. Sharawi, "Printed multi-band MIMO antenna systems and their performance metrics [wireless corner]," *IEEE Antennas Propag. Mag.*, vol. 55, no. 5, pp. 218–232, Oct. 2013.

WEI HU (S'09–M'13) received the Ph.D. degree in electromagnetic fields and microwave technology from Xidian University, Xi'an, China, in 2013. From 2013 to 2017, he was a Lecturer with the National Key Laboratory of Antennas and the Microwave Technology, Collaborative Innovation Center of Information Sensing and Understanding, Xidian University, where he is currently an Associate Professor. From 2018 to 2019, he visited the University of Kent, U.K., as an Academic Visitor. He has authored and coauthored more than 40 internationally refereed journal articles and has been serving as a Reviewer for a number of technical journals and international conferences. His current research interests include multiband and wideband antennas, circularly polarized antennas, MIMO antenna arrays, and wideband wide-scanning phased arrays.

LONG QIAN received the B.S. degrees from Xidian University, Xi'an, China, in 2017, where he is currently pursuing the M.S. degree in electromagnetic field and microwave technology with the National Laboratory of Science and Technology on Antennas and Microwaves. His research interests include mobile terminal antennas and 5G/sub-6GHz MIMO antennas for wireless applications.

STEVEN GAO (M'01–SM'16–F'19) received the Ph.D. degree in microwave engineering from Shanghai University, China. He is currently a Full Professor and the Chair in RF and microwave engineering, and the Director of Graduate Studies, School of Engineering and Digital Arts, University of Kent, U.K. He coauthored/co-edited three books such as *Space Antenna Handbook* (Wiley, 2012), *Circularly Polarized Antennas* (IEEE-Wiley, 2014), and *Low-Cost Smart Antennas* (Wiley, 2019), more than 300 articles and ten patents. His research interests include smart antennas, phased arrays, MIMO, reconfigurable antennas, wideband/multiband antennas, satellite antennas, RF/microwave/mm-wave/THz circuits, mobile communications, satellite communications, UWB radars, synthetic-aperture radars, The IoT, and sensors for healthcare. He is a Fellow of Royal Aeronautical Society, U.K., and the IET, U.K. He was a General Chair of LAPC 2013, and an Invited Speaker at many conferences. He was a Distinguished Lecturer of the IEEE AP Society, and is an Associate Editor of the IEEE TRANSACTIONS ON ANTENNAS AND PROPAGATION and several other international Journals, such as *Radio Science*, the IEEE ACCESS, *Electronics Letters*, *IET Circuits*, and *Devices and Systems*, and the Editor-in-Chief for John Wiley & Sons Book Series on *Microwave and Wireless Technologies*.

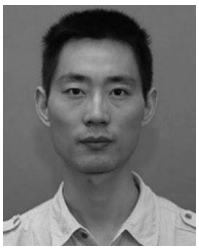

LE-HU WEN received the M.S. degree from Xidian University, Xi'an, China, in 2011. He is currently pursuing the Ph.D. degree with the University of Kent, Canterbury, U.K. His current research interests include multiband base station antenna, mobile terminal antenna, and tightly coupled array.

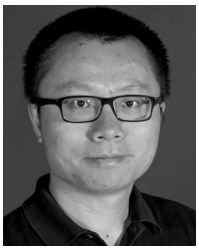

QI LUO (S'08–M'12) received the Ph.D. degree (Hons.) from the University of Porto, Portugal, in 2012. He is currently with the School of Engineering and Digital Arts, University of Kent, U.K., as a Research Fellow. He authored/coauthored two books, *Circularly Polarized Antennas* (Wiley-IEEE, 2014) and *Low-Cost Smart Antennas* (Wiley, 2019). He also authored a book chapter in *Handbook of Antenna Technologies* (Springer, 2014). His research interests include smart antennas, circularly polarized antennas, reflectarray, transmitarray, multiband microstrip antennas, and electrically small antennas. He was awarded as the Outstanding Reviewer for the IEEE TRANSACTIONS ON ANTENNAS AND PROPAGATION, in 2015.

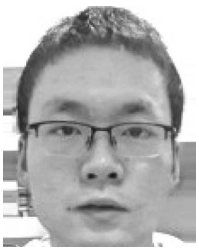

HANG XU received the Ph.D. degree from the University of Kent, Canterbury, U.K., in 2019. He is currently an Antenna Engineer with Huawei Technologies Company Ltd., Shenzhen, China. His research interests include 5G smartphone antennas, MIMO antenna arrays, decoupling technology, microwave and millimeter-wave antennas, and base station antennas.

XUEKANG LIU received the B.S. degree in electronic and information engineering from Xidian University, Xi'an, China, in 2016, where he is currently pursuing the M.S. degree in electromagnetic fields and microwave technology. His current research interests include wideband antennas, multimode antennas, and omnidirectional antennas.

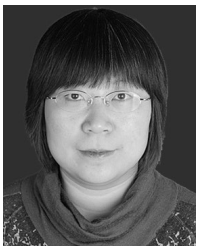

YING LIU (M'09–SM'16) received the M.S. and Ph.D. degrees in electromagnetics from Xidian University, Xi'an, China, in 2001 and 2004, respectively. From 2006 to 2007, she was a Postdoctoral Researcher with Hanyang University, Seoul, South Korea. She is currently a Full Professor and the Director of the National Key Laboratory of Science and Technology on Antennas and Microwaves, Xidian University. She has authored or coauthored more than 100 refereed journal articles. She is the author of *Prediction and Reduction of Antenna Radar Cross Section* (Xi'an: Xidian University Press, 2010) and *Antennas for Mobile Communication Systems* (Beijing: Electronics Industry Press, 2011). Her research interests include antenna theory and technology, prediction, and control of antenna RCS. Dr. Liu is a Senior Member of Chinese Institute of Electronics. She is a Reviewer of several international journals and serves as a TPC Member or a Session Chair for several IEEE flagship conferences. She was a recipient of the New Century Excellent Talents in University of the Ministry of Education for China, in 2011.

WEI WANG received the Ph.D. degree in electrical engineering from Shanghai University, Shanghai, China, in 2005. From 1993 to 1998, he was an Assistant Engineer with the East China Research Institute of Electronic Engineering (ECRIEE), Hefei, where he was an Engineer, from 2001 to 2002. He is currently a Research Professor with ECRIEE. He has authored and coauthored more than 50 journal articles and 60 conference papers. He holds 30 Chinese patents. His current research interests include waveguide slot antennas, microstrip antennas for radar, compact ultrawideband for wireless communications, microwave passive devices and circuits, and microwave/millimeter systems. Dr. Wang is a Senior Member of the Chinese Institute of Electronics, Beijing, China. He was a recipient of many awards, including one Second Class Award for Scientific and Technology of National Progress, two Second Class Awards for Scientific and Technology Progress of National Defense Industry, one First Class and one Third Class Awards for scientific and technology achievements in China Electronic Technology Group Corporation, one First Class Award for Electronic Information Science and Technology of China Electronic Institute, and one First Class and one Second Class Awards for Excellent Academic Papers in Natural Science of Anhui Province.